Acta Biomaterialia 18 (2015) 9–20

Contents lists available at ScienceDirect

Acta Biomaterialia

journal homepage: www.elsevier.com/locate/actabiomat

Effect of calcium phosphate coating and rhBMP-2 on bone regeneration in rabbit calvaria using poly(propylene fumarate) scaffolds

Mahrokh Dadsetan [a,1], Teja Guda [b,1], M. Brett Runge [a], Dindo Mijares [c], Racquel Z. LeGeros [c], John P. LeGeros [c], David T. Silliman [d], Lichun Lu [a], Joseph C. Wenke [d], Pamela R. Brown Baer [d], Michael J. Yaszemski [a,*]

[a] Biomaterials and Tissue Engineering Laboratory, Mayo Clinic, Rochester, MN, USA
[b] Department of Biomedical Engineering, University of Texas at San Antonio, San Antonio, TX, USA
[c] Department of Biomaterials & Biomimetics, New York University, New York, NY, USA
[d] United States Army Institute of Surgical Research, Fort Sam Houston, TX, USA

ARTICLE INFO

Article history:
Received 29 May 2014
Received in revised form 9 December 2014
Accepted 24 December 2014
Available online 7 January 2015

Keywords:
Bone regeneration
Poly(propylene fumarate)
Calcium phosphate coating
Rabbit calvarial defect
3-D printing

ABSTRACT

Various calcium phosphate based coatings have been evaluated for better bony integration of metallic implants and are currently being investigated to improve the surface bioactivity of polymeric scaffolds. The aim of this study was to evaluate the role of calcium phosphate coating and simultaneous delivery of recombinant human bone morphogenetic protein-2 (rhBMP-2) on the in vivo bone regeneration capacity of biodegradable, porous poly(propylene fumarate) (PPF) scaffolds. PPF scaffolds were coated with three different calcium phosphate formulations: magnesium-substituted β-tricalcium phosphate (β-TCMP), carbonated hydroxyapatite (synthetic bone mineral, SBM) and biphasic calcium phosphate (BCP). In vivo bone regeneration was evaluated by implantation of scaffolds in a critical-sized rabbit calvarial defect loaded with different doses of rhBMP-2. Our data demonstrated that scaffolds with each of the calcium phosphate coatings were capable of sustaining rhBMP-2 release and retained an open porous structure. After 6 weeks of implantation, micro-computed tomography revealed that the rhBMP-2 dose had a significant effect on bone formation within the scaffolds and that the SBM-coated scaffolds regenerated significantly greater bone than BCP-coated scaffolds. Mechanical testing of the defects also indicated restoration of strength in the SBM and β-TCMP with rhBMP-2 delivery. Histology results demonstrated bone growth immediately adjacent to the scaffold surface, indicating good osteointegration and osteoconductivity for coated scaffolds. The results obtained in this study suggest that the coated scaffold platform demonstrated a synergistic effect between calcium phosphate coatings and rhBMP-2 delivery and may provide a promising platform for the functional restoration of large bone defects.

1. Introduction

In both military and civilian populations, treatment of large segmental bone defects remains an unsolved clinical challenge, despite a wide array of existing bone graft materials. The synthetic bone graft strategies used to treat large traumatic defects usually consist of a combination of osteoconductive scaffolds that provide mechanical stability and deliver osteoinductive growth factors to recruit osteogenic cells to induce regeneration. These scaffolds should mimic bone morphology, structure and function in order to optimize integration into surrounding tissue. Bone is a structure composed of hydroxyapatite crystals deposited within an organic matrix consisting of ~95% type I collagen [1]. Morphologically, bone is composed of trabecular bone which creates a porous environment with 50–90% porosity and pore sizes of 1 mm in diameter with cortical bone surrounding it [2]. In terms of bone architecture and composition, porous structural scaffolds with osteoconductive surfaces loaded with growth factors are suitable platforms to optimize accelerated functional bone regeneration. Mechanical strength is an important property of scaffolds being considered for the replacement of load-bearing bone. Scaffold mechanical properties are strongly influenced by internal architecture and must be carefully designed. Many porous ceramic scaffolds produced to date have exhibited strengths in the range 10–30 MPa. The mechanical strengths of human trabecular bone in proximal tibia and distal femur have been reported to be in the range of 1.8–63.6 and 413–1516 MPa, respectively [3]. By manipulating overall porosity, the strength can be adjusted to match site-specific requirements.

* Corresponding author. Tel.: +1 507 284 3747; fax: +1 507 284 5075.
E-mail address: yaszemski.michael@mayo.edu (M.J. Yaszemski).
[1] Both these authors contributed equally to the preparation of this manuscript.

http://dx.doi.org/10.1016/j.actbio.2014.12.024
1742-7061/

Report Documentation Page

Form Approved
OMB No. 0704-0188

1. REPORT DATE	2. REPORT TYPE	3. DATES COVERED
01 MAY 2015	**N/A**	**-**

4. TITLE AND SUBTITLE	5a. CONTRACT NUMBER
Effect of calcium phosphate coating and rhBMP-2 on bone regeneration in rabbit calvaria using poly(propylene fumarate) scaffolds	5b. GRANT NUMBER
	5c. PROGRAM ELEMENT NUMBER
6. AUTHOR(S)	5d. PROJECT NUMBER
Dadsetan M., Guda T., Runge B. M., Mijares D., LeGeros R. Z., LeGeros J. P., Silliman D. T., Lu L., Wenke J. C., Brown Baer P. R., Yaszemski M. J.,	5e. TASK NUMBER
	5f. WORK UNIT NUMBER
7. PERFORMING ORGANIZATION NAME(S) AND ADDRESS(ES)	8. PERFORMING ORGANIZATION REPORT NUMBER
United States Army Institute of Surgica; Research, JBSA Fort Sam Houston, TX 78234	
9. SPONSORING/MONITORING AGENCY NAME(S) AND ADDRESS(ES)	10. SPONSOR/MONITOR'S ACRONYM(S)
	11. SPONSOR/MONITOR'S REPORT NUMBER(S)

12. DISTRIBUTION/AVAILABILITY STATEMENT
Approved for public release, distribution unlimited

13. SUPPLEMENTARY NOTES

14. ABSTRACT

15. SUBJECT TERMS

16. SECURITY CLASSIFICATION OF:			17. LIMITATION OF ABSTRACT	18. NUMBER OF PAGES	19a. NAME OF RESPONSIBLE PERSON
a. REPORT	b. ABSTRACT	c. THIS PAGE			
unclassified	**unclassified**	**unclassified**	**SAR**	**12**	

Standard Form 298 (Rev. 8-98)
Prescribed by ANSI Std Z39-18

Changes in macroporosity have been shown to affect mechanical properties more than changes in microporosity.

Poly(propylene fumarate) (PPF) is a photo-cross-linkable or chemical cross-linkable polyester that has been studied extensively for treatment of bone defects either as an injectable in situ curing material [4,5] or as preformed scaffolds [6–10]. Preformed scaffolds with high porosity allow bone ingrowth while providing the structural support required for stability and space maintenance during the treatment of segmental bone defects. Scaffolds with very complex 3-D architectures and predetermined size, shape and porosity can be fabricated using solid freeform fabrication (SFF) through computer-aided design (CAD) [8,9,11,12].

PPF is particularly suited for these applications because of its mechanical properties and has previously been optimized for rapid prototyping by UV laser stereolithography [8]. The creation of functional composite scaffolds that mimic the bone extracellular matrix by pairing polymeric matrices with bioactive coatings has been shown to direct biomineralization and stimulate cell adhesion, proliferation and differentiation. Specifically, hydroxyapatite and other calcium phosphate coatings have been studied extensively to better integrate biomaterial implants with bone for applications such as hip replacement [13,14], dental implants [15,16] and screws for fracture fixation [17,18]. These coatings provide a bone-like mineral matrix that simulates the in vivo bone environment [19], and are a prerequisite for the attachment of osteoblasts and possibly drive osteogenic differentiation of adult stem cells. Calcium phosphate coatings adsorb many proteins and other macromolecules, leading to a biological layer that favors cell attachment and osteogenic differentiation. Additionally, it has been shown that the osteoinductive efficacy of recombinant human bone morphogenetic protein-2 (rhBMP-2) can be enhanced when incorporated with calcium phosphate coatings [11,20,21]. Thus, the application of calcium phosphate coatings on the surface of porous polymeric scaffolds may allow for increased osteoconductivity and potentially improved osteoinductivity with the delivery of suitable growth factors, allowing for improved bone regeneration in vivo.

In this study, the effect of three calcium phosphate coating materials on 3-D PPF scaffolds loaded with different doses of rhBMP-2 have been characterized in vitro and evaluated in vivo for their bone regeneration potential. To the best of our knowledge, there is no study on the effect of these calcium phosphate formulations on in vivo osseointegration of coated polymeric implants. The three calcium phosphate coating formulations selected, magnesium-substituted β-tricalcium phosphate (β-TCMP), carbonate hydroxyapatite (synthetic bone mineral, SBM) and biphasic calcium phosphate (BCP), each has unique properties that promote osseointegration and bioactivity both in vitro and in vivo [22,23]. Incorporation of Mg in the β-TCMP formulation provides stability to the Ca–P bond similar to biological systems, reflected in the resistance of this coating to hydrolysis [24]. Mg appears to stabilize the beta-tricalcium phosphate (β-TCP) structure due to increased electrostatic bonding of Mg–O compared to Ca–O. Synthetic bone mineral (SBM) mimics the mineral phase of natural bone, described as carbonate apatite [22,25]. This coating includes Mg^{2+} and Zn^{2+} ions that are shown to suppress osteoclastic resorption in vitro and promote osteoblastic activity (bone formation) in vitro and in vivo [26]. Biphasic calcium phosphate (BCP) consists of an intimate mixture of hydroxyapatite (HA) and β-TCP, with varying HA/β-TCP ratios. BCP is a promising biomaterial for bone reconstruction that supports osteogenesis [23,27,28]. The BCP used in this study includes HA and β-TCP at a ratio of 80:20.

In this study, by combining a porous scaffold of PPF that provides mechanical stability with three unique calcium phosphate coatings and rhBMP-2 at three doses (0, 50 and 100 μg per scaffold), the objective was to evaluate which coating and at what growth factor dose functional bone healing in a rabbit calvarial model could be achieved over 6 weeks.

2. Methods

2.1. PPF synthesis and scaffold fabrication

All reagents were purchased from Aldrich and used as received unless otherwise noted. PPF (Mn = 1900, PDI = 1.96) was synthesized from diethyl fumarate (DEF) and 1,2-propanediol catalyzed by $ZnCl_2$ according to previously published methods [29]. PPF was dissolved in DEF at a ratio of 60:40 (w/w) by heating at 50 °C until completely dissolved. 1.5 wt.% of the photoinitiator bisphenyl(2,4,6-trimethylbenzyol) phosphine oxide was added to the resin. Cylindrical 3-D PPF scaffolds with dimensions of 15.2 mm diameter × 2.5 mm height were fabricated using a Viper si2 stereolithography system (3D Systems, Valencia, CA) using parameters determined in previously published procedures [8]. After fabrication scaffolds were washed with 3 ml acetone and extensively with ethanol to remove excess resin before post-curing in a UV chamber (3D Systems, Valencia, CA). PPF scaffolds were extracted by Soxhlet extraction with tetrahydrofuran for 48 h.

2.2. Calcium phosphate coatings

β-TCMP and SBM were coated on PPF scaffolds in a chemical bath using a precipitation-type method. In an attempt to cause the actual occurrence of β-TCMP on the surface of the scaffold in repeated layers, each scaffold was immersed in refreshed solutions for 10 min of solution A and then in solution B for ten cycles each of A and B (i.e. a total of 100 min in solution A and 100 min in solution B). Solution A consists of 0.05 M calcium acetate ($Ca(C_2H_3O_2)_2$) and 0.05 M magnesium acetate ($Mg(C_2H_3O_2)_2$) and solution B is 0.05 M NaH_2PO_4 shaken for 10 min at 60 °C. After 10 cycles, scaffolds transferred into a mixture of solution A and solution B (50:50, v/v) and aged at 60 °C for 4 days. Aging solution was refreshed every 24 h. SBM coating was performed in solution A containing 0.0013 M $ZnCl_2$, 0.0025 M $MgCl_2{\cdot}6H_2O$ and 0.01 M $CaCl_2$, and in solution B containing 0.0007 M NaF, 0.01 M $NaHCO_3$ and 0.005 M K_2HPO_4 under the same conditions described above for β-TCMP coating. Hence, the bonding between the polymer surface and minerals might be due to a thin layer coating mechanism. BCP was coated on scaffold surfaces with pretreatment of the scaffolds in acetone for 5 min and vortex for 2 min in biphasic calcium phosphate with an HA/β-TCP ratio of 80:20.

2.3. Scanning electron microscopy (SEM), energy dispersive X-ray spectroscopy (EDAX) and thermogravimetric analysis (TGA)

To examine the coating morphology and composition on scaffolds, specimens were sputter coated with Au/Pd followed by imaging using a S-4700 scanning electron microscope (Hitachi-High Tech, Tokyo, Japan). Samples for EDAX were mounted onto carbon double-sided sticky tape and left uncoated. Specimens were placed in the scanning electron microscope which was operated at 20 kV. Spectra were collected at a magnification of 5000× for 100 s using a System SIX™ EDS microanalysis system (Thermo Noran, Middleton, WI).TGA was performed on a TA Q500 thermal analyzer at a heating rate of 5 °C min^{-1} from 5 to 800 °C under flowing nitrogen.

2.4. Porosity measurement with micro-computed tomography (micro-CT)

Four scaffolds per group were scanned using a SkyScan 1076 micro-CT system (Bruker-MicroCT, Kontich, Belgium) at 8.87 μm

spatial resolution. The reconstruction thresholds were chosen using the Otsu thresholding algorithm [30] applied across all the samples to minimize error. Morphometric analysis was carried out on CT images using CTanalyzer v. 1.4 (Bruker-MicroCT, Kontich, Belgium). In order to determine scaffold strut organization, traditional histomorphometric parameters were computed for each of the scaffolds over the entire 3-D volume. The parameters computed were scaffold volume ratio (SV/TV), strut thickness (St. Th) and strut spacing (St. Sp). Additionally, 3-D volume models of the scaffolds were generated from the micro-CT scans using Mimics (v. 13.0, Materialise NV, Leuven, Belgium).

2.5. rhBMP-2 loading, in vitro release kinetics and biological activity

rhBMP-2 (Humanzyme, Chicago, IL) with the weight of 0, 50 and 100 μg per scaffold surfaces, using bovine collagen solution as a delivery vehicle for implantation in rabbit calvarial defects. The rhBMP-2 doses were chosen based on a previously published paper on rat femoral defects [31]. Briefly, 40 μl bovine collagen solution (3 mg ml^{-1}) was mixed with 20 μl of rhBMP-2 solution (5 mg ml^{-1}) in a sterile centrifuge tube and added to scaffolds. Scaffolds were placed in sterile tissue culture plates and air-dried in a tissue culture hood prior to implantation. However, for studies of loading efficiency and release kinetics, a dose of 50 μg was used. The controlled release kinetics was determined by incubating the loaded PPF scaffolds in phosphate-buffered saline (PBS) at 37 °C for 42 days. The media was collected at different time periods and rhBMP-2 release was measured using an ELISA kit (R&D Systems, Minneapolis, MN).

The biological activity of released rhBMP-2 was assessed using rabbit bone marrow stromal cells (MSCs). All animal surgery in this study for cell isolation was performed according to a protocol approved by the Mayo Clinic Institutional Animal Care and Use Committee (IACUC). Using bilateral ileac crest puncture, MSCs were harvested from 2 month old New Zealand White rabbits. When the cultures were 85% confluent (~14 days), the cells were released from the dish with 0.25% trypsin–EDTA and replated at 250,000 cells per 75 mm plate. MSCs were cultured in low-glucose Dulbecco's modified Eagle's medium (DMEM) supplemented with 10% fetal bovine serum (FBS), and 1% penicillin/streptomycin. For rhBMP-2 biological activity, MSCs were plated at a density of 2×10^4 cells cm^{-2} on 24-well tissue culture plates. After 24 h of incubation at 37 °C, the media in each well was replaced with osteogenic media supplemented with 2 μg ml^{-1} of either exogenous rhBMP-2 or rhBMP-2 released from PPF scaffolds. The alkaline phosphatase (ALP) activity of the cells in the presence of exogenous rhBMP-2 (control) or released from the scaffolds were determined after 3 days of treatment. The ALP activity of seeded cells at desired time points was measured according to the manufacturer's instructions (Sigma). Briefly, at the end of treatment, the cells were rinsed twice with PBS. Alkaline lysis buffer (0.3 ml, 0.75 M 2-amino-2-methyl-1-propanol, pH 10.3) containing *p*-nitrophenol phosphate substrate (2 mg ml^{-1}) was added and the mixture was incubated for 30 min at 37 °C. To stop the reaction, 0.3 ml 50 mM NaOH was added. The samples and standards were diluted in 20 mM NaOH, and the absorbance was measured at 409 nm. ALP activity was normalized to total cellular protein which was determined by the Bradford protein assay (Bio-Rad, Hercules, CA).

2.6. Rabbit surgery and animal care

All animal surgeries in this study were conducted in compliance with the Animal Welfare Act, the implementing Animal Welfare Regulations, and the principles of the Guide for the Care and Use of Laboratory Animals. To assess the healing potential of the PPF scaffold materials with three different calcium phosphate coatings (β-TCMP, SBM, BCP) and three rhBMP-2 doses (0, 50 and 100 μg), a 15 mm critical-sized defect [32] was created in adult female New Zealand White rabbits (n = 10). To reduce intraoperative pain and induce a surgical plane of anesthesia, buprenorphine hydrochloride (0.03 mg kg^{-1}), ketamine (35 mg kg^{-1}) and xylazine (5 mg kg^{-1}) were administered intramuscularly followed by isoflurane (1–3%) delivered in 100% oxygen (flow rate 3–5 l min^{-1} for induction and 1.5–1.75 l min^{-1} for maintenance) through a laryngeal mask airway. Following general anesthesia induction and surgical site preparation, a midline coronal surgical incision was made and the tissues were dissected to expose the calvaria. Using a surgical drill with a trephine supplemented with physiological saline for irrigation, a craniotomy (15 mm in diameter) was prepared in the midline of the calvaria in the parietal bones. Coated PPF scaffolds were inserted into the craniotomies according to the experimental plan and soft tissues were closed in layers with resorbable 3-0 sutures. To control post-operative pain a 25 μg h^{-1} transdermal fentanyl patch was affixed to the shaved dorsum of the rabbit.

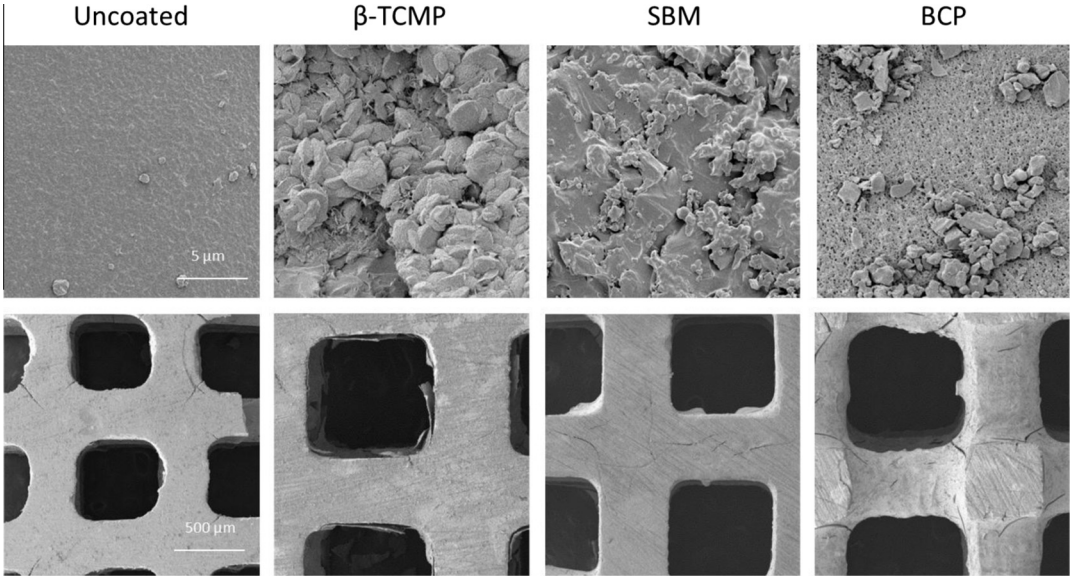

Fig. 1. SEM images of different calcium phosphate coated scaffolds compared to the uncoated PPF scaffold show a rough surface for coated scaffolds while the pore structure remains open after coating.

The rabbits were recovered and survived for 6 weeks, at which time the calvarial samples containing the healed defects were harvested post euthanasia and fixed in 10% formalin.

2.7. Micro-CT analysis

Each specimen was placed on the scanning platform of a GE eXplore Locus micro-CT (GE Healthcare, Wauwatosa, WI) and 360 X-ray projections were collected (80 kVp; 500 mA; 26 min total scan time). Projection images were preprocessed and reconstructed into 3-D volumes (20 μm resolution) using a modified tent-FDK cone beam algorithm (GE reconstruction software). These images were then converted to a bitmap sequence using ImageJ 1.44p (US National Institutes of Health, Bethesda, MD). DataViewer (Bruker-MicroCT, Kontich, Belgium) was used to realign the bitmap images such that the principal axes of the image

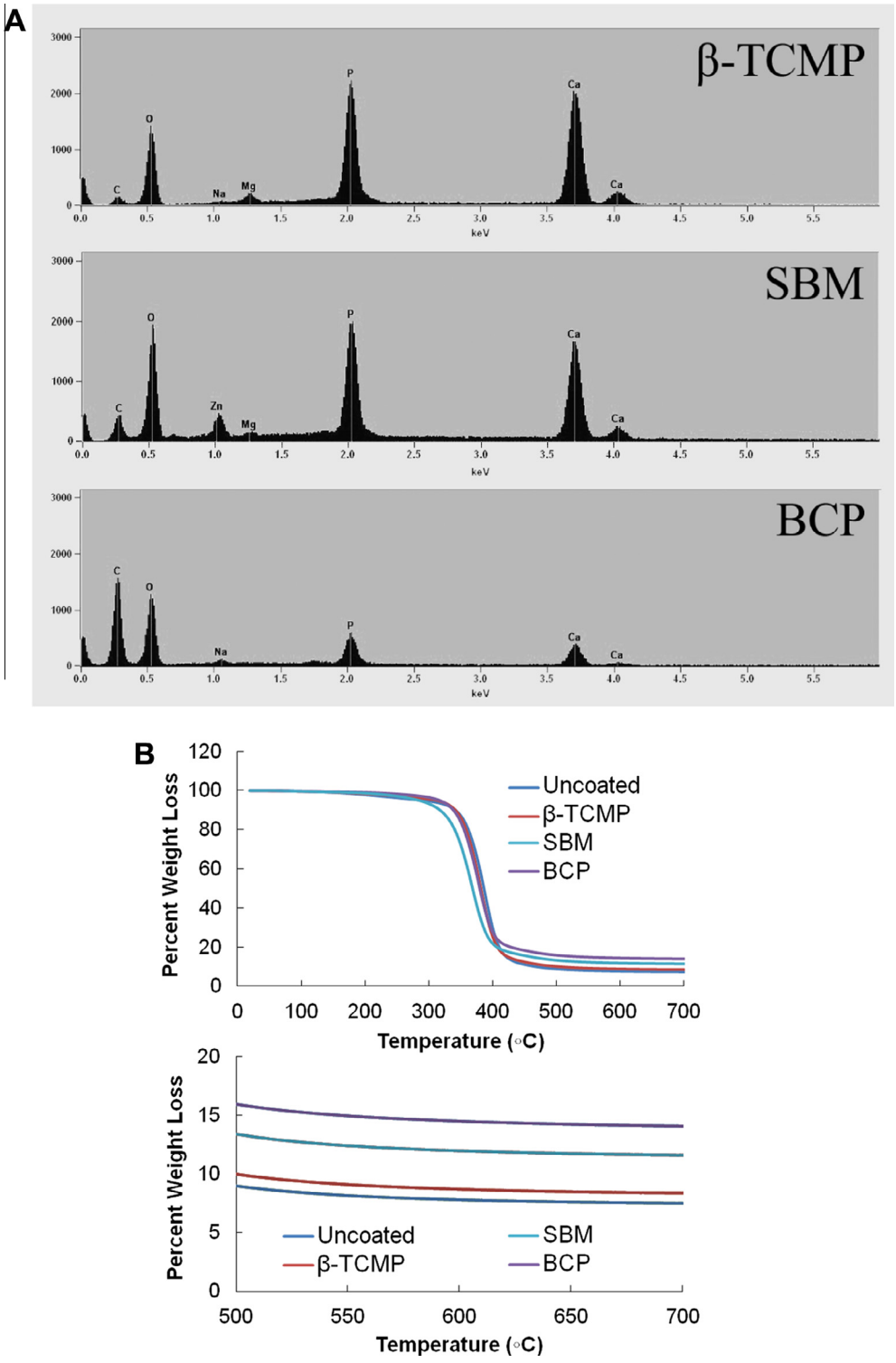

Fig. 2. (A) EDAX shows calcium and phosphate peaks on the surface of coated scaffolds. Calcium phosphate peak intensities on β-TCMP and SBM were greater than on BCP. (B) TGA confirmed the presence of minerals on PPF scaffolds. There was ~1–5% mineral on scaffold surfaces. The bottom panel is a blow up of the TGA thermogram (upper panel) showing the weight remaining between 0 and 20%.

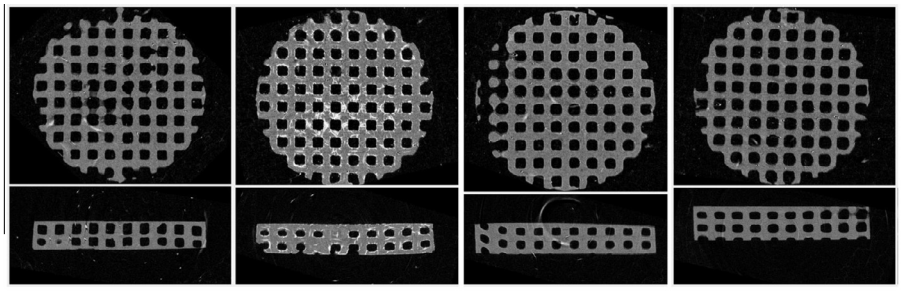

		Uncoated	BTCMP	SBM	BCP	
Bone Volume/ Tissue Volume	BV/TV	34.76 ± 0.85	40.17 ± 2.16	38.79 ± 1.58	39.13 ± 0.88	%
Trabecular Thickness	Tb.Th	526.7 ± 6.7	529.4 ± 1.4	504.6 ± 12.2	541.4 ± 12.1	μm
Trabecular Spacing	Tb.Sp	484.7 ± 24.4	353.6 ± 20.7	403.0 ± 18.9	429.2 ± 11.0	μm

Fig. 3. Representative micro-CT cross-sections showing the pore architecture of the PPF scaffolds without coating and with each of three different calcium phosphate coatings. The β-TCMP coating alone was clearly visible in micro-CT images as bright white.

Table 1
PPF scaffold porosity and architecture measured by micro-CT before and after different calcium phosphate coatings.

	Uncoated	β-TCMP	SBM	BCP
Scaffold volume/total volume (%)	34.8 ± 0.8	40.2 ± 2.2	38.8 ± 1.6	39.1 ± 0.9
Strut thickness (μm)	526.7 ± 6.7	529.4 ± 1.4	504.6 ± 12.2	541.4 ± 12.1
Strut spacing (μm)	484.7 ± 24.4	353.6 ± 20.7	403.0 ± 18.9	429.2 ± 11.0

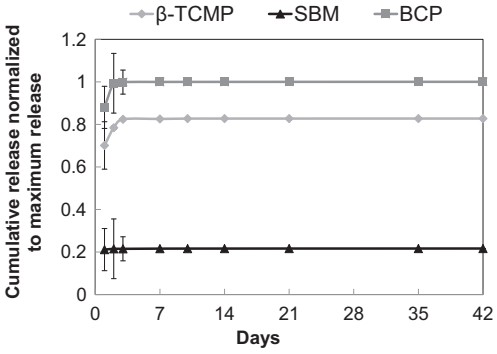

Fig. 4. Controlled release kinetics of rhBMP-2 from 3-D PPF scaffolds with three different calcium phosphate coatings. A burst release over the first 3 days for both β-TCMP and BCP was observed. However, only 20% of the rhBMP-2 was released from the scaffolds coated with SBM, almost all of it in an immediate burst release.

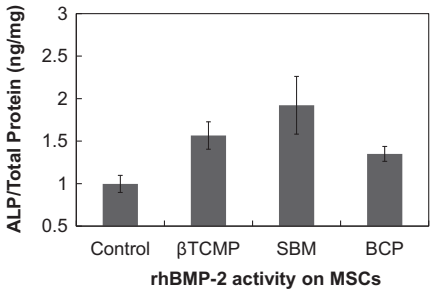

Fig. 5. rhBMP-2 released from all scaffolds remained biologically active. Biological activity was assessed by measurement of ALP activity of MSCs exposed to the released BMP. Cells directly treated with exogenous BMP used as control. No significant differences were found between groups.

were aligned to the principal axes of the calvarial defect. The samples were then thresholded globally using the Otsu algorithm across all the groups in the study. The 15 mm defect created was then located to define the region of interest by identifying the space occupied by the scaffold to distinguish defect edges. This region was 3.5 mm thick and its thickness was centered to account for the native curvature of the calvarium. 3-D volume (bone volume to total volume ratio), bone mineral density and morphometric analysis was carried out on CT images using CT analyzer v. 1.4 as previously described [33]. The relative distribution of trabecular thickness was calculated as the fraction of trabeculae at each trabecular thickness (in steps of 40 μm). Bone mineral density of the regenerated bone tissue was normalized to the mineral density of the native calvarial bone to evaluate the quality and maturity of the bone tissue regenerated. In order to determine the effect of the scaffold's porous architecture on the infiltration of new bone tissue, depth profiles of the bone area filled in each cross-section of the calvarial defect from the superior to the inferior (dural) interface were generated. 3-D volume models of the regenerated bone within the defect were generated from the micro-CT scans using Mimics for qualitative visualization of spatial connectivity.

2.8. Histological analysis

All samples were processed and analyzed in the Biomaterials and Characterization Histomorphometry Core Laboratory at the Mayo Clinic using undecalcified processing. Each specimen was dehydrated, embedded in methacrylate and polymerized. Sections 5 μm thick were cut using a Leica RM 2265 microtome and stained using Gomori's Trichrome. Complete histology slide images were acquired at 20× magnification using an Eclipse 55i microscope, DS-Fi1 Camera and compiled using the NIS Elements Imaging Software BR 4.10.01 (all from NikInstruments Inc., Melville, NY) and analyzed using Photoshop (v. 7.0.1, Adobe

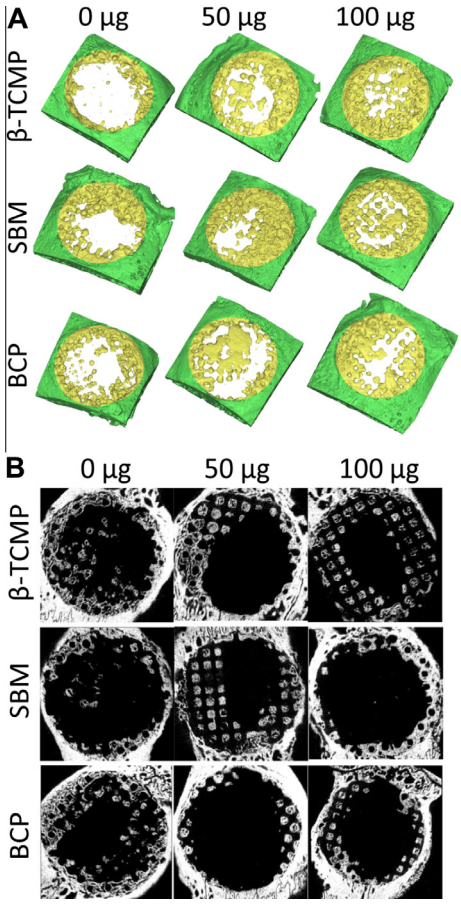

Fig. 6. (a) Representative 3-D renderings of micro-CT images of in vivo defects showing regenerated mineralized tissue in yellow and surrounding native calvarial bone in green. (b) Axial-cross section of the same representative scaffolds from each group after 6 weeks of implantation in defects.

Systems Inc., San Jose, CA). Using Photoshop, the defect area and the PPF scaffold were defined manually. In addition, color thresholding (selecting for the blue/teal stain) was used to define the mineralized tissue within the defect. Pixel quantification was used to calculate the areas of the defect, PPF scaffold and the mineralized tissue separately. The percentage available space mineralized was calculated as the ratio of the mineralized tissue to the defect area minus the scaffold [mineralized tissue/(defect area − scaffold area)].

2.9. Mechanical push-out testing

Specimens were stored in buffered formalin solution and refrigerated until testing (6 samples per experimental group plus 6 control calvaria). Specimens were allowed to equilibrate to room temperature before testing was conducted. A custom fixture which included a 6.2 mm flat indenter and a rigid platform with an 8.5 mm hole was mounted on a servohydraulic test machine (858 MiniBionix II, MTS Systems, Eden Prairie, MN) instrumented with a 1000 N load cell. Calvaria specimens were placed on the fixture platform, resting the superior face of the calvarium on the platform and centering the circular defect of the dural face with the indenter axis. Care was also taken to align the face of the defect to be parallel to the indenter face. Under displacement control, the indenter was forced into the repair zone surface at a rate of 5 mm min^{-1} until failure and continuing until a total displacement of 7.5 mm was reached. MATLAB (2013a, MathWorks, Natick, MA) was used to identify the peak compressive force for each set of data.

2.10. Statistical analysis

All data are represented as mean ± standard error of the mean. Significance in biological activity of rhBMP-2 delivered and porosity of scaffolds post-coating was determined using a one-way ANOVA (across coating type) and Tukey's test for post hoc evaluation when significance was found. In the case of ex vivo measurement of micro-CT parameters, histological morphometry and push-out strength, a two-way ANOVA (across coating type and rhBMP-2 dose) and Tukey's test for post hoc evaluation was employed. Within the push-out strength data, Grubbs' test was used to determine outliers within each group by the extreme Studentized deviate method at a two-tailed significance of $P < 0.05$ and one sample from two groups was ignored as an outlier. Significance level was set at$P < 0.05$ for all statistical measures reported. Statistical analysis was carried out using SigmaPlot (v. 11.0, Systat Software, Inc., San Jose, CA).

3. Results

3.1. Scaffold and coating characterization

3-D PPF scaffolds with 1000 μm pore size and 500 μm wall thicknesses were fabricated via a stereolithography technique using UV crosslinking at a wavelength of 355 nm. The SEM images in Fig. 1 show that PPF surface morphology changed after coating with calcium phosphate. The scaffold surfaces appear to be rougher in comparison to PPF without coating and crystal-like materials are seen on the surface of scaffolds. The most significant changes due to coating are observed on scaffolds with β-TCMP coating. The β-TCMP coating appears to be thicker and some chipping and flaking can be seen on the surface of scaffolds with this coating material. In addition, the SEM images at higher magnification reveal that the scaffold pore sizes are slightly smaller than 1000 μm. This could be due to thermal effect of the long-wavelength UV light (355 nm) used in the stereolithography system which results in overcuring of the resin. The pore sizes remain unchanged after coating with different calcium phosphate formulations. Elemental analysis using EDAX showed strong Ca and P peaks on the surface of scaffolds coated with SBM and β-TCMP, while these peaks were smaller on scaffolds coated with BCP, indicating less mineral coverage on this group of scaffolds (Fig. 2A). Quantitative analysis of coatings with TGA showed a weight remaining of 13% > 9% > 8.2% for scaffolds coated with β-TCMP, SBM, BCP, respectively, after thermal degradation at 700 °C (Fig. 2B). A weight remaining of 8.1 ± 1.0% was observed for uncoated PPF.

3.2. Scaffold micro-CT evaluation

3-D reconstructions of all scaffolds showed good geometric control over scaffold struts and an even pattern of pores and struts in accordance with the material design (Fig. 3). Micro-CT analysis showed that the scaffold porosity ranged between 60% and 65% across all groups. However, no significant difference was observed between scaffolds in terms of scaffold volume ratio (SV/TV, $P = 0.224$) and strut thickness (St. Th., $P = 0.115$). In terms of strut spacing (St. Sp.), it was observed that the β-TCMP group (354 μm) had significantly smaller spacing ($P = 0.004$) than the uncoated scaffold (485 μm) (Table 1). The micro-CT analysis was able to detect an evident coating in only the β-TCMP group, as shown in Fig. 3 by the bright pattern (calcium phosphate being

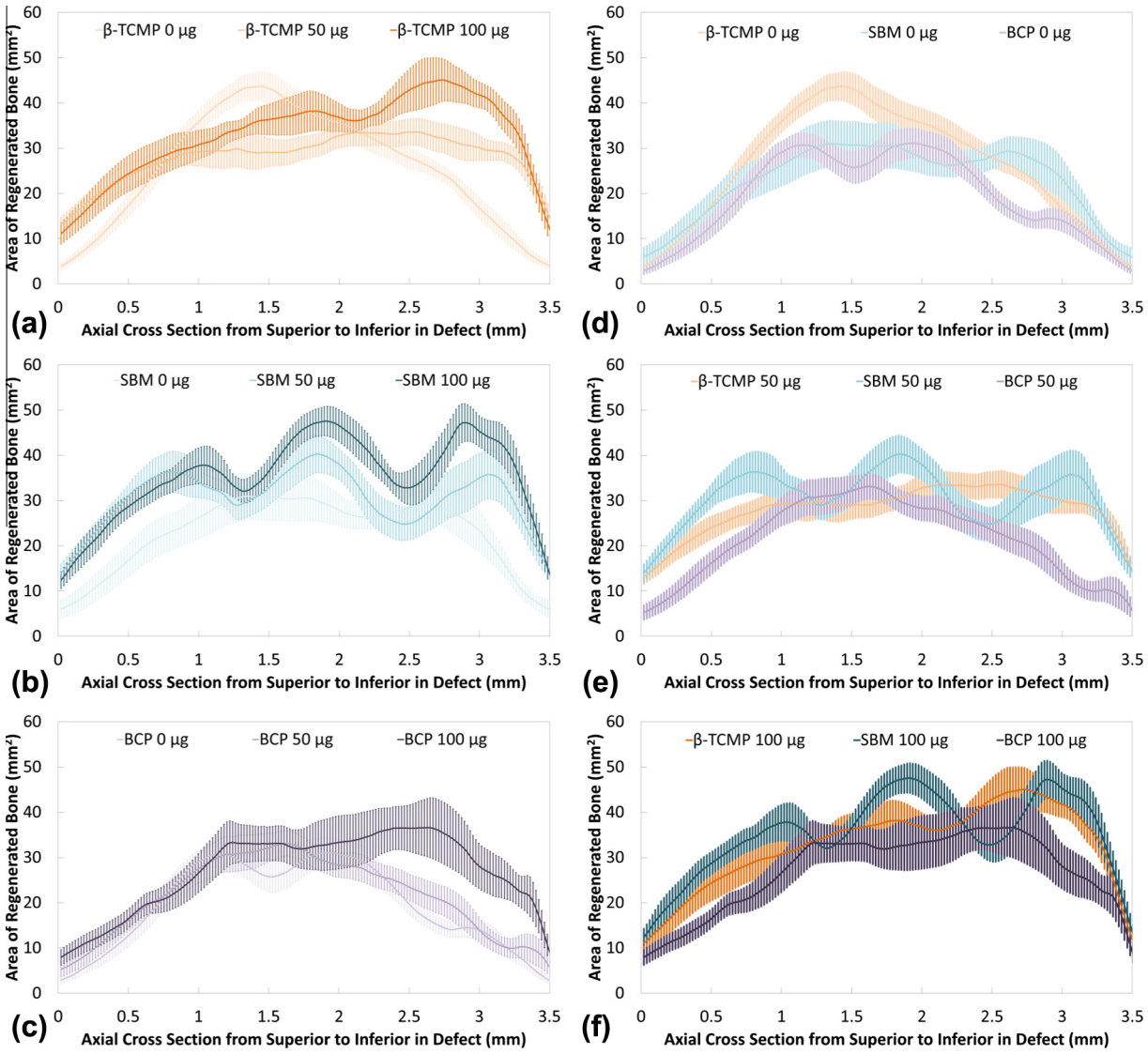

Fig. 7. Graphical representation of bone area filled per defect cross-section along the depth of the defect within each scaffold type (a–c) at each rhBMP-2 dose (d–f). Without rhBMP-2, the three groups demonstrate a bone-healing response biased towards the superior side of the defect. At the high 100 μg rhBMP-2 dose, a clear bias towards greater bone regeneration on the inferior side (dural side) of the scaffolds was observed.

denser than the polymeric scaffold) distributed across the scaffold cross-section.

3.3. rhBMP-2 loading, release kinetics and biological activity in vitro

Fifty μg rhBMP-2 was loaded onto PPF scaffolds using bovine collagen solution (3 mg ml^{-1}). The controlled release kinetics was determined by incubating the loaded PPF scaffolds in PBS at 37 °C for 42 days. The media was collected at different time periods and BMP release was measured using an ELISA kit. The data, which appear in Fig. 4, show a burst release over the first 3 days for both the magnesium-substituted TCP (β-TCMP) and the TCP/HA blend (biphasic calcium phosphate, BCP). However, only 20% of the BMP was released from the scaffolds that were coated with SBM (carbonate hydroxyapatite). Moreover, measurements of the ALP activity of MSCs revealed that rhBMP-2 released from all scaffolds remained biologically active. The released rhBMP-2 biological activity was similar to the biological activity of MSCs exposed to exogenous rhBMP2 (control) (Fig. 5).

3.4. Ex vivo micro-CT evaluation

Micro-CT analysis revealed that bone regeneration occurred throughout the scaffolds. The regenerated bone originated both from the native bone at the defect margins as well as at locations completely interior to the scaffold (Fig. 6A). The coverage of the defect within the 3-D reconstructions showed a trend of increasing bone formation with rhBMP-2 dose delivered ($P < 0.001$ as a main effect). Additionally, from the micro-CT cross-sectional images, bone was observed to regenerate in an organized pattern that was similar to the pore space of the PPF scaffolds (negative template) with bridging observed within the channels connecting pores (Fig. 6B). This observation was also supported by the multiple peaks/fronts observed in the bone area distribution along the depth of the scaffolds from the superior to the dural side of the defect. This effect is seen most distinctly in the SBM coating group, where three distinct peaks are observed ~1 mm apart, which matches the spacing between pores/struts on the PPF scaffolds (Fig. 7). Without rhBMP-2, all three scaffold groups showed bone regeneration biased towards the superior aspect of the scaffold,

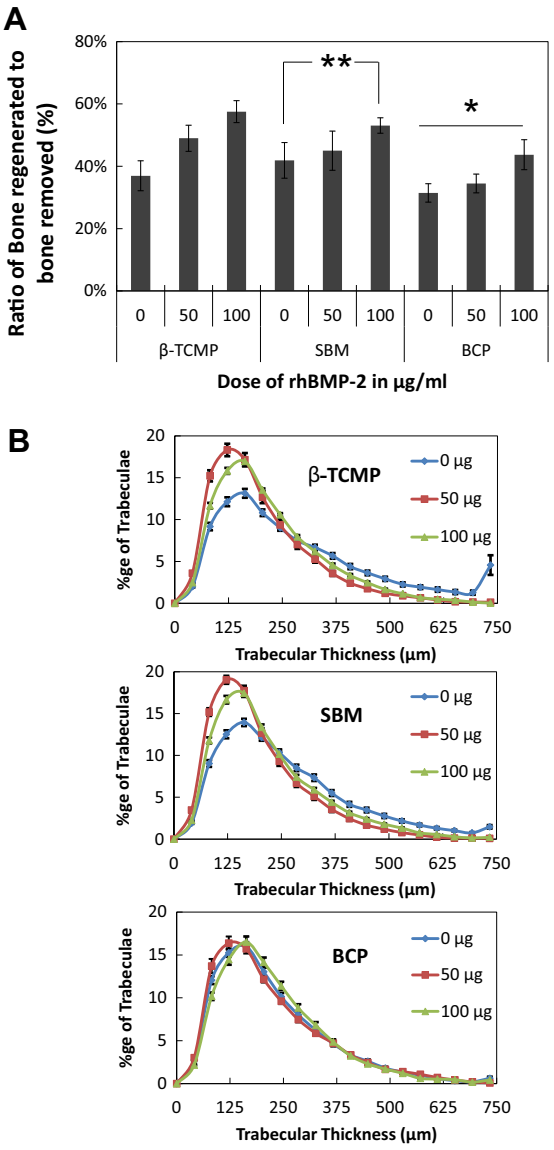

Fig. 8. (A) Total regenerated bone volume in specimens, expressed as a percentage of bone volume removed to create the defect. BCP was significantly lower than other materials across all doses (indicated by $^{*}P < 0.02$). The 100 µg dose regenerated significantly greater bone than no rhBMP-2 (indicated by $^{**}P < 0.01$) in the SBM group. Across groups, the 100 µg dose regenerated significantly greater amounts of bone than both other rhBMP-2 doses ($P = 0.05$). (B) Relative distribution of trabecular thickness of regenerated bone trabeculae at each rhBMP-2 dose for each different coating.

most clearly observed in the β-TCMP-coated scaffolds. The distribution of regenerated bone was relatively uniform across scaffold depth at the 50 µg rhBMP-2 dose, while at the 100 µg dose, a clear bias in bone regeneration was observed towards the dural aspect of the defect. This phenomenon was most clearly observed in the β-TCMP- and SBM-coated scaffolds (Fig. 7).

For quantitative analysis from micro-CT reconstructions, the bone volume regenerated in each defect at 6 weeks was normalized to the total bone volume removed during defect creation at surgery. From this analysis, it was observed that the 100 µg rhBMP-2 dose regenerated significantly greater bone than the no rhBMP-2 dose ($P < 0.001$) as well as the 50 µg rhBMP-2 dose across all groups ($P = 0.049$). Additionally, the βTCMP- and SBM-coated groups both performed significantly better than the BCP group at bone regeneration across all rhBMP-2 doses ($P = 0.016$) (Fig. 8A). In terms of bone mineral density, it was observed that the regenerated bone mineral density was significantly higher when no rhBMP-2 was delivered (118 ± 1% that of native calvarial density) compared to when 50 µg (112 ± 1%) and 100 µg (114 ± 1%) rhBMP-2 doses were delivered across all coatings ($P = 0.041$). Comparing the scaffolds without rhBMP-2, it was observed that the bone mineral density was significantly higher ($P = 0.004$) with the β-TCMP coating (123 ± 2%) compared to the BCP coating (113 ± 2%). Trabecular thickness distributions indicated that without rh-BMP2 delivery, the β-TCMP coating showed a few large trabeculae. With 50 and 100 µg rhBMP-2, an increase in the relative number of trabeculae was observed in the 40–200 µm range for both the β-TCMP- and SBM-coated scaffolds (Fig. 8B). It was also observed that the trabecular distribution of all three coatings at the 100 µg rhBMP-2 dose was very similar. Unlike the β-TCMP- and SBM-coated groups, there was no change in the relative distribution of trabecular thickness with rhBMP-2 dose within the BCP-coated group (Fig. 8B).

3.5. Ex vivo histological evaluation

Normal cellular infiltration and bone healing was observed across all scaffold treatment groups and no signs of persistent inflammatory response were observed (Fig. 9). In addition, bone regeneration was observed in direct contact with the scaffold surface, with visible osteoblasts and blood vessel infiltration (Fig. 9B). A dose response of bone regenerated to rhBMP-2 delivery was observed in the defects treated with the βTCMP and BCP scaffolds. Within the single central histological cross-section, morphometric analysis indicated that the SBM scaffolds loaded with rhBMP-2 (50 and 100 µg) regenerated significantly greater bone within the available pore space than the scaffolds without rhBMP-2 ($P < 0.001$). Additionally, a group effect was noted, with SBM scaffolds regenerating significantly greater bone within the open pore space than the β-TCMP- and BCP-coated scaffolds for all rhBMP-2 doses (Fig. 10A, $P = 0.031$). No significant differences in scaffold area were observed across the three different coatings and the different rhBMP-2 doses (Fig. 10B, $P = 0.678$). As anticipated, similar trends of bone area regenerated relative to total tissue area (Fig. 10B) were observed between experimental groups as in the case of bone area relative to open pore area (Fig. 10A) within the histological section.

3.6. Ex vivo push-out strength

Functional testing of the regenerated bone strength was carried out by push-out testing. It was observed that the β-TCMP-coated group showed significantly greater ($P = 0.038$) push-out strength than the SBM-coated group across the different rhBMP-2 doses (Fig. 11). The push-out strength of the coatings with the 100 µg rhBMP-2 dose was significantly higher than that of the groups with the 0 and 50 µg rhBMP-2 doses ($P = 0.027$) across all three coating materials. No difference was found within the BCP-coated scaffolds with different rhBMP-2 doses (82 ± 6 N, $P = 0.828$). The β-TCMP coating with the 100 µg rhBMP-2 dose was the strongest group tested (132 ± 10 N) and was significantly stronger than the β-TCMP-coated scaffolds with 0 and 50 µg rhBMP-2 doses ($P = 0.019$). By comparison, the strength of the native intact calvarial controls was found to be 340 ± 52 N.

4. Discussion

Calcium phosphate coatings to improve bioactivity of implants that are in contact with bone [13–18] as well as to improve osteoconductivity of scaffolds for bone regeneration [11,34–38] have

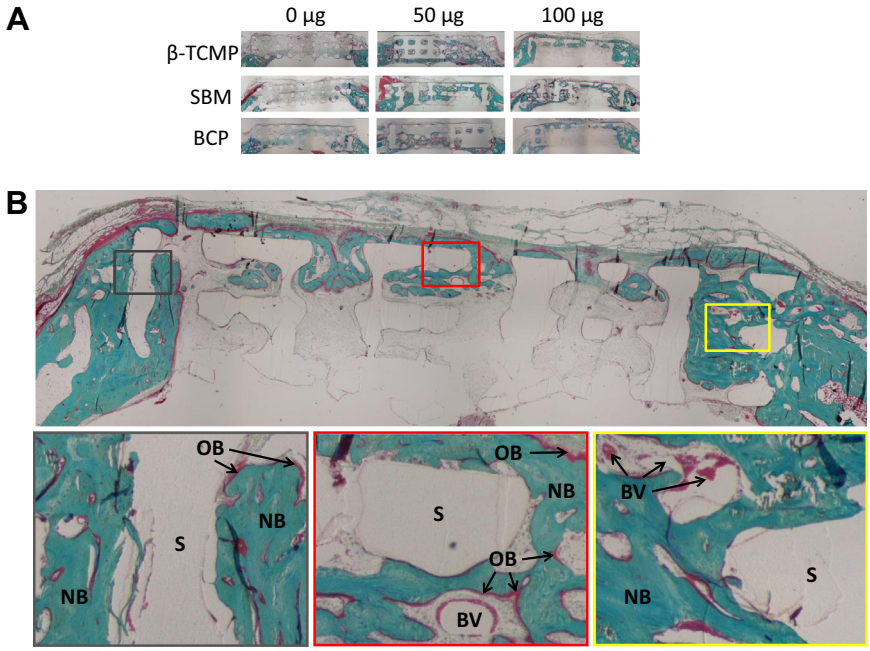

Fig. 9. (A) Histology of scaffolds with three different calcium phosphate coatings and 0, 50 or 100 μg rhBMP-2 loadings. In these images the purple stain represents osteoid and green stain indicates new bone formation (Gomori's Trichrome). (B) Representative histological image from a β-TCMP scaffold with 100 μg rhBMP-2 showing magnified insets at either interface and in the center of the defect. Labels indicate: scaffold (S), new bone (NB), blood vessel (BV) and osteoblasts (OB). Color codes (black, red and yellow) are used to indicate the correlation of the histogram region with the magnified image.

been widely investigated. However, extensive in vivo studies comparing the relative efficacy of different calcium phosphate coatings for bone regeneration both with and without the delivery of growth factors are relatively scarce [39,40]. In the current study, we used porous PPF scaffolds manufactured via SFF to compare three different bioactive calcium phosphate coatings, β-TCMP, SBM and BCP, in terms of their bone regenerative capacity in vivo both with and without different doses of rhBMP-2. PPF is a promising polymer for bone tissue engineering because its mechanical and degradation properties can be tailored for specific applications. It has also been shown to be bone biocompatible in different rats and rabbits [41,42]. Multiple factors affect the regeneration of bone observed in the scaffolds at 6 weeks including the bioactivity of the coatings and the influence of the rhBMP-2.

Past studies have noted that given the strong affinity of rhBMP-2 to bind strongly to calcium phosphate coatings, ~10% [11,43] to 50% [44] of the delivered rhBMP-2 dose might remain surface bound on the coating and that the phase composition and surface structure of the calcium phosphate determine the extent of rhBMP-2 binding [45]. The role played by this surface-bound rhBMP-2 has not been clearly identified [43], though it has been suggested that it influences apatite formation and bone regeneration at the micro-scale [46]. The difference between the release kinetics of rhBMP-2 in our study could be due to difference in coating chemical composition. It was observed that the SBM-coated scaffolds only released 20% of the rhBMP-2 loaded while the β-TCMP- and BCP-coated groups showed significantly greater release (Fig. 4). The interaction between protein molecules and the hydroxyapatite crystals is an important research topic. However, the nature of their non-covalent bonding is still not clear at the atomic level. A previous study has shown that both the phase composition and calcium phosphate microstructure affect binding capacity for bone-related proteins such as BMP-2 and thus lead to the difference in their osteoinduction and release profile [45]. Three types of adsorption functional groups, $-OH$, $-NH_2$ and $-COO^-$, are required for protein BMP-2 to interact with HA surface, while most experiments with other proteins have find only one of these, i.e. the $-COO^-$ group. As mentioned above, SBM coating consists of a calcium carbonate apatite (similar to bone apatite) matrix incorporating Mg^{2+} and Zn^{2+} and F^- ions [47]. Therefore, the slower BMP-2 release could be due to strong bonding between BMP-2 functional groups and positively charged ions on the SBM [48]. Over the duration of the in vivo model in the current study (6 weeks), the SBM group did not show significant differences from the other two groups, indicating that the additional rhBMP-2 might not have been released over this duration. Future studies using slow release or strongly binding calcium phosphates should consider the long-term effects of its release and the biological activity of the bound rhBMP-2. From the micro-CT results, it was observed that the SBM-coated scaffolds loaded with rhBMP-2 (either 50 or 100 μg) regenerated significantly greater bone volume (BV/TV) than BCP-coated scaffolds loaded with rhBMP-2. This observation is in line with previous reports of surface-based regeneration of bone [46] and suggests that the potential role of bound rhBMP-2 to calcium phosphate coatings bears further investigation to enhance scaffold osteoinductivity, especially since it has been reported that the local concentration of calcium ions increases this affinity while phosphate ions inhibit it [48,49].

The coatings were extensively characterized prior to implantation to understand the differences between materials, and regenerated bone quality, quantity and functionality were assessed ex vivo to identify potential correlations regarding the relative efficacy of each coating technique. From micro-CT analysis of the coated scaffolds, no differences were observed between the different coating techniques in terms of overall scaffold porosity or architecture as measured by strut thickness and separation. SEM images qualitatively indicate differences in the surface roughness of the coatings, and surface topography has been extensively studied for its effects on osteogenic cells with rougher surfaces causing increased cellular activity, differentiation and matrix production [50]. The BCP-coated scaffolds which had the least surface roughness after coating were observed to regenerate significantly less bone after

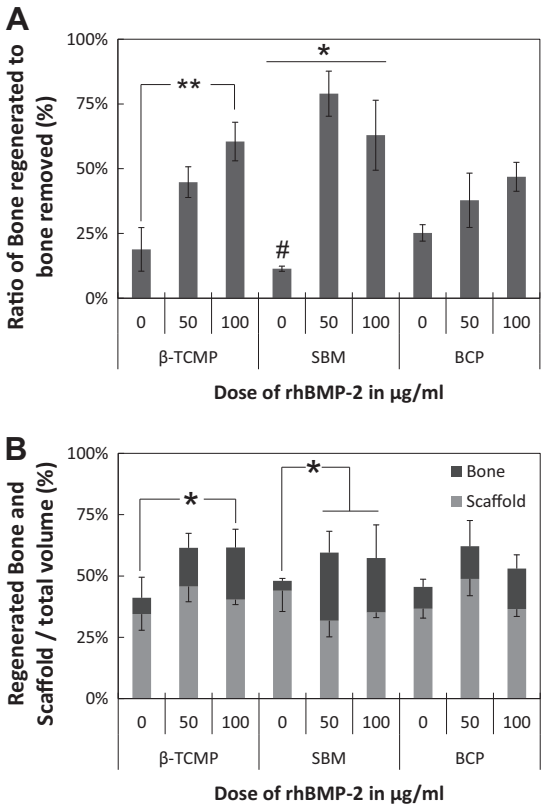

Fig. 10. (A) Total regenerated bone area in specimens, expressed as a percentage of bone area removed to create the defect. Data are presented as the average ± SEM. The SBM group regenerated significantly greater amounts bone for all rhBMP-2 doses (indicated by $^{*}P < 0.05$) though the 0 µg dose was significantly lower than the other two rhBMP-2 doses within the SBM group (indicated by $^{\#}P < 0.001$). The 100 µg dose regenerated greater bone than the 0 µg dose within the β-TCMP scaffolds ($^{**}P < 0.01$). (B) Regenerated bone area and residual scaffold area in specimens, expressed as a percentage of bone area removed to create the defect. No significant difference in scaffold area was observed between groups across different rhBMP-2 doses. Significant differences in bone area regenerated are indicated by $^{*}P < 0.05$. The bone area filled within the SBM group was significantly higher than the BCP group for all the rhBMP-2 doses ($P < 0.05$), while both rhBMP-2 doses regenerated significantly higher bone than the no rhBMP-2 control for all scaffold types ($P < 0.001$).

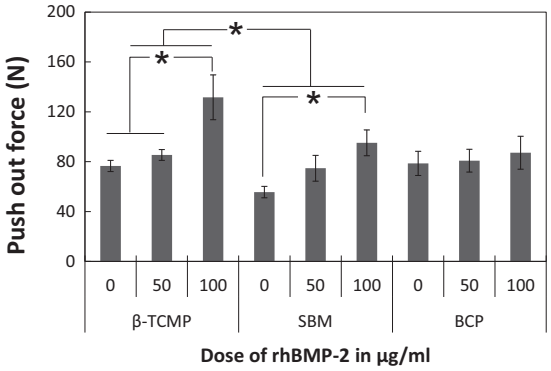

Fig. 11. Push-out strength of the calvarial regenerated bone. Data are presented as average ± SEM, and significant differences indicated by $^{*}P < 0.05$. Additionally, at the 100 µg dose of rhBMP-2, the β-TCMP scaffolds had the highest push-out strength, significantly higher than the SBM and BCP scaffolds ($P < 0.05$). No significant difference was observed in push-out strength of BCP scaffolds with or without rhBMP-2.

6 weeks implantation compared to the other two groups, but given the number of confounding variables between the nine groups in the study, it is difficult to show direct causality. This could be due to incorporation of Mg and Zn in β-TCMP and SBM as shown by elemental analysis and a low mineral content on BCP scaffolds [18,26]. It has been shown that some trace minerals are important in maintaining bone quality due to their role in the synthesis of collagen and other bone proteins. For example, Zn regulates secretion of calcitonin from the thyroid gland, influences bone turnover and causes a reduction in osteoclastic activity, collagen synthesis and ALP activity as well as stimulating bone formation [51].

The considerable bone regeneration observed within all scaffolds with no rhBMP-2 delivery in a critical-sized defect at 6 weeks indicates that all three calcium phosphate coatings were osteoconductive. This is further supported by the histological observations of bone growing immediately adjacent to the scaffold surface with no intervening fibrous tissue observed and no signs of sustained inflammatory response after 6 weeks. These results seem to indicate that the scaffold coatings enhance osseointegration and minimize potential inflammatory response to scaffold degradation and polymer breakdown as compared to bare polymeric scaffolds [42]. Additionally, the controlled architecture and large size of the pores seems to significantly enhance the degree of bone infiltration compared to previous studies (<3% bone infiltration) on PPF scaffolds with a more random pore organization [41].

Analysis of trabecular thickness also indicated that the delivery of 50 and 100 µg of rhBMP-2 did not significantly change the relative distribution of trabeculae regenerated within the defect in the BCP-coated scaffolds. This also indicates that with an appropriate calcium phosphate coating the osteoinductive effect of rhBMP-2 can be enhanced. Therefore, lower doses of rhBMP-2 were required in this study compared to those recommended (260 µg for a 15 mm rabbit calvaria) in our previous work [52]. The spatial profiles of bone regeneration indicated that the SBM scaffold best directed bone regeneration into the scaffold pores as indicated by three distinct fronts aligned with the pores of the SFF printed scaffold (Fig. 7). It is also interesting to note that the scaffolds without rhBMP-2 seemed to have a superior bias to bone regeneration while the scaffolds with the 100 µg rhBMP-2 dose seemed to demonstrate an inferior (dural) bias to bone regeneration. This trend could be attributed either to which stabilizing callus formed first or to the source of the osteogenic cells that regenerated the defect.

Unlike a load-bearing critical-sized defect model in which bone healing is influenced by mechanical load, in a calvarial defect model the ability of composite scaffolds and growth factor is investigated solely in terms of bone healing and integration [53]. Thus, the push-out test provides the most functional evaluation of the integration of the scaffold with the native calvaria [54]. The push-out force for native calvarial bone was significantly higher (340 N) than the best performing group in the study (β-TCMP with 100 µg BMP2, 132 N) after 6 weeks of implantation. Other comparable studies in the rabbit calvarial model evaluated the push-out strength after a minimum of 12 weeks' implantation [55,56] and additionally tested 15 mm bilateral defects in the calvarium. It is possible that the significantly higher native bone strength in our study compared to previous studies (180 N [55,56]) is due to testing across the sagittal suture as opposed to within the thin shell of the parietal bone. No difference in push-out strength was observed within the different rhBMP-2 doses in the BCP-coated scaffolds, while the β-TCMP group had significantly higher push-out strength at the 100 µg rhBMP-2 dose than the BCP group. Changes in bone volume and strength over time were not considered in this study as it was anticipated that the differences between coatings would be most prominent at an early time point. Future studies should consider the effect of scaffold degradation paired with increased regeneration on the overall restoration of strength and increase in area coverage of the defect [57].

5. Conclusions

In this work, we demonstrated that 3-D PPF scaffolds in combination with calcium phosphate coating can perform as a platform for bone regeneration in a calvarial defect. Among the three coatings studied, β-TCMP and SBM in combination with rhBMP-2 improved osteoconductivity and osteointegration of porous PPF at lower than recommended rhBMP-2 doses. The BCP coating did not offer any particular advantage in terms of the quantity, quality or function of regenerated bone in the rabbit calvaria. Therefore, our findings in this study suggest the added benefit of using enhanced calcium phosphate coated PPF scaffolds for use in the treatment of bone defects.

Acknowledgments

This work was supported by the Mayo Foundation, NIH grant R01 EB03060 and Armed Forces Institute of Regenerative Medicine award number W81XWH-08-2-0034.

Appendix A. Figures with essential color discrimination

Certain figures in this article, particularly Figs. 2, 6 and 8–10, are difficult to interpret in black and white. The full color images can be found in the on-line version, at http://dx.doi.org/10.1016/j.actbio.2014.12.024.

References

[1] Karageorgiou V, Kaplan D. Porosity of 3D biomaterial scaffolds and osteogenesis. Biomaterials 2005;26:5474–91.
[2] Cooper DML, Matyas JR, Katzenberg MA, Hallgrimsson B. Comparison of microcomputed tomographic and microradiographic measurements of cortical bone porosity. Calcif Tissue Int 2004;74:437–47.
[3] Goldstein SA. The mechanical properties of trabecular bone: dependence on anatomic location and function. J Biomech 1987;20:1055–61.
[4] Kempen DH, Lu L, Kim C, Zhu X, Dhert WJ, Currier BL, et al. Controlled drug release from a novel injectable biodegradable microsphere/scaffold composite based on poly(propylene fumarate). J Biomed Mater Res A 2006;77:103–11.
[5] Kim CW, Talac R, Lu L, Moore MJ, Currier BL, Yaszemski MJ. Characterization of porous injectable poly-(propylene fumarate)-based bone graft substitute. J Biomed Mater Res A 2008;85A:1114–9.
[6] Kempen DH, Kruyt MC, Lu L, Wilson CE, Florschutz AV, Creemers LB, et al. Effect of autologous bone marrow stromal cell seeding and bone morphogenetic protein-2 delivery on ectopic bone formation in a microsphere/poly(propylene fumarate) composite. Tissue Eng A 2008;15:587–94.
[7] Lee K-W, Wang S, Dadsetan M, Yaszemski MJ, Lu L. Enhanced cell ingrowth and proliferation through three-dimensional nanocomposite scaffolds with controlled pore structures. Biomacromolecules 2010;11:682–9.
[8] Lee K-W, Wang S, Fox BC, Ritman EL, Yaszemski MJ, Lu L. Poly(propylene fumarate) bone tissue engineering scaffold fabrication using stereolithography: effects of resin formulations and laser parameters. Biomacromolecules 2007;8:1077–84.
[9] Lee K-W, Wang S, Lu L, Jabbari E, Currier BL, Yaszemski MJ. Fabrication and characterization of poly(propylene fumarate) scaffolds with controlled pore structures using 3-dimensional printing and injection molding. Tissue Eng 2006;12:2801–11.
[10] Wang S, Lu L, Yaszemski MJ. Bone-tissue-engineering material poly(propylene fumarate): correlation between molecular weight, chain dimensions, and physical properties. Biomacromolecules 2006;7:1976–82.
[11] Al-Munajjed AA, O'Brien FJ. Influence of a novel calcium-phosphate coating on the mechanical properties of highly porous collagen scaffolds for bone repair. J Mech Behav Biomed Mater 2009;2:138–46.
[12] Lee JW, Lan PX, Kim B, Lim G, Cho D-W. Fabrication and characteristic analysis of a poly(propylene fumarate) scaffold using micro-stereolithography technology. J Biomed Mater Res B Appl Biomater 2008;87B:1–9.
[13] Geesink R, de Groot K, Klein C. Bonding of bone to apatite-coated implants. J Bone Joint Surg Br 1988;70-B:17–22.
[14] Yang Y, Kim K-H, Ong JL. A review on calcium phosphate coatings produced using a sputtering process—an alternative to plasma spraying. Biomaterials 2005;26:327–37.
[15] Hayakawa T, Yoshinari M, Kiba H, Yamamoto H, Nemoto K, Jansen JA. Trabecular bone response to surface roughened and calcium phosphate (Ca–P) coated titanium implants. Biomaterials 2002;23:1025–31.
[16] Nguyen HQ, Deporter DA, Pilliar RM, Valiquette N, Yakubovich R. The effect of sol–gel-formed calcium phosphate coatings on bone ingrowth and osteoconductivity of porous-surfaced Ti alloy implants. Biomaterials 2004;25:865–76.
[17] Hyup Lee J, Ryu H-S, Lee D-S, Sun Hong K, Chang B-S, Lee C-K. Biomechanical and histomorphometric study on the bone-screw interface of bioactive ceramic-coated titanium screws. Biomaterials 2005;26:3249–57.
[18] Xu L, Pan F, Yu G, Yang L, Zhang E, Yang K. In vitro and in vivo evaluation of the surface bioactivity of a calcium phosphate coated magnesium alloy. Biomaterials 2009;30:1512–23.
[19] LeGeros RZ. Properties of osteoconductive biomaterials: calcium phosphates. Clin Orthop Relat Res 2002:81–98.
[20] Wu G, Hunziker EB, Zheng Y, Wismeijer D, Liu Y. Functionalization of deproteinized bovine bone with a coating-incorporated depot of BMP-2 renders the material efficiently osteoinductive and suppresses foreign-body reactivity. Bone 2011;49:1323–30.
[21] Wu G, Liu Y, Iizuka T, Hunziker EB. The effect of a slow mode of BMP-2 delivery on the inflammatory response provoked by bone-defect-filling polymeric scaffolds. Biomaterials 2010;31:7485–93.
[22] Daculsi G, LeGeros RZ, Heughebaert M, Barbieux I. Formation of carbonate-apatite crystals after implantation of calcium phosphate ceramics. Calcif Tissue Int 1990;46:20–7.
[23] Daculsi G, Legeros RZ, Nery E, Lynch K, Kerebel B. Transformation of biphasic calcium phosphate ceramics in vivo: ultrastructural and physicochemical characterization. J Biomed Mater Res 1989;23:883–94.
[24] Legeros RZ, Sakae T, Bautista C, Retino M, Legeros JP. Magnesium and carbonate in enamel and synthetic apatites. Adv Dent Res 1996;10:225–31.
[25] Sader MS, Martins VCA, Gomez S, LeGeros RZ, Soares GA. Production and in vitro characterization of 3D porous scaffolds made of magnesium carbonate apatite (MCA)/anionic collagen using a biomimetic approach. Mater Sci Eng C 2013;33:4188–96.
[26] LeGeros R, Bleiwas C, Retino M, Rohanizadeh R, LeGeros J. Zinc effect on the in vitro formation of calcium phosphates: relevance to clinical inhibition of calculus formation. Am J Dent 1999;12:65–71.
[27] Bouler J-M, LeGeros RZ, Daculsi G. Biphasic calcium phosphates: influence of three synthesis parameters on the HA/β-TCP ratio. J Biomed Mater Res 2000;51:680–4.
[28] LeGeros RZ, Lin S, Rohanizadeh R, Mijares D, LeGeros JP. Biphasic calcium phosphate bioceramics: preparation, properties and applications. J Mater Sci Mater Med 2003;14:201–9.
[29] Wang S, Lu L, Gruetzmacher JA, Currier BL, Yaszemski MJ. A Biodegradable and cross-linkable multiblock copolymer consisting of poly(propylene fumarate) and Poly(ε-caprolactone): synthesis, characterization, and physical properties. Macromolecules 2005;38:7358–70.
[30] Otsu N. A threshold selection method from gray-level histograms. Automatica 1975;11:23–7.
[31] Boerckel JD, Kolambkar YM, Dupont KM, Uhrig BA, Phelps EA, Stevens HY, et al. Effects of protein dose and delivery system on BMP-mediated bone regeneration. Biomaterials 2011;32:5241–51.
[32] Hollinger JO, Kleinschmidt JC. The critical size defect as an experimental model to test bone repair materials. J Craniofac Surg 1990;1:60–8.
[33] Guda T, Darr A, Silliman DT, Magno MHR, Wenke JC, Kohn J, et al. Methods to analyze bone regenerative response to different rhBMP-2 doses in rabbit craniofacial defects. Tissue Eng Part C Methods 2014;20:749–60.
[34] Ciapetti G, Ambrosio L, Savarino L, Granchi D, Cenni E, Baldini N, et al. Osteoblast growth and function in porous poly ε-caprolactone matrices for bone repair: a preliminary study. Biomaterials 2003;24:3815–24.
[35] Kim S-H, Oh S-A, Lee W-K, Shin US, Kim H-W. Poly(lactic acid) porous scaffold with calcium phosphate mineralized surface and bone marrow mesenchymal stem cell growth and differentiation. Mater Sci Eng C 2011;31:612–9.
[36] Kim S-S, Park MS, Gwak S-J, Choi CY, Kim B-S. Accelerated bonelike apatite growth on porous polymer/ceramic composite scaffolds in vitro. Tissue Eng 2006;12:2997–3006.
[37] Rezwan K, Chen QZ, Blaker JJ, Boccaccini AR. Biodegradable and bioactive porous polymer/inorganic composite scaffolds for bone tissue engineering. Biomaterials 2006;27:3413–31.
[38] Yang F, Wolke JGC, Jansen JA. Biomimetic calcium phosphate coating on electrospun poly(ε-caprolactone) scaffolds for bone tissue engineering. Chem Eng J 2008;137:154–61.
[39] Barrere F, van Blitterswijk CA, de Groot K. Bone regeneration: molecular and cellular interactions with calcium phosphate ceramics. Int J Nanomed 2006;1:317–32.
[40] Yuan H, Yang Z, de Bruijn JD, de Groot K, Zhang X. Material-dependent bone induction by calcium phosphate ceramics: a 2.5-year study in dog. Biomaterials 2001;22:2617–23.
[41] Fisher JP, Vehof JWM, Dean D, van der Waerden JPCM, Holland TA, Mikos AG, et al. Soft and hard tissue response to photocrosslinked poly(propylene fumarate) scaffolds in a rabbit model. J Biomed Mater Res 2002;59:547–56.
[42] Hedberg EL, Kroese-Deutman HC, Shih CK, Crowther RS, Carney DH, Mikos AG, et al. In vivo degradation of porous poly(propylene fumarate)/poly(DL-lactic-co-glycolic acid) composite scaffolds. Biomaterials 2005;26:4616–23.
[43] Winn SR, Uludag H, Hollinger JO. Sustained release emphasizing recombinant human bone morphogenetic protein-2. Adv Drug Deliv Rev 1998;31:303–18.
[44] Autefage H, Briand-Mésange F, Cazalbou S, Drouet C, Fourmy D, Gonçalvès S, et al. Adsorption and release of BMP-2 on nanocrystalline apatite-coated and

uncoated hydroxyapatite/β-tricalcium phosphate porous ceramics. J Biomed Mater Res B Appl Biomater 2009;91B:706–15.
[45] Wang J, Zhang H, Zhu X, Fan H, Fan Y, Zhang X. Dynamic competitive adsorption of bone-related proteins on calcium phosphate ceramic particles with different phase composition and microstructure. J Biomed Mater Res B Appl Biomater 2013;101B:1069–77.
[46] Lan Levengood SK, Polak SJ, Poellmann MJ, Hoelzle DJ, Maki AJ, Clark SG, et al. The effect of BMP-2 on micro- and macroscale osteointegration of biphasic calcium phosphate scaffolds with multiscale porosity. Acta Biomater 2010;6:3283–91.
[47] Mijares D, Kulkarni A, Lewis K, Yao F, Xi Q, Tannous S, et al. Oral bone loss induced by mineral deficiency in a rat model: effect of a synthetic bone mineral (SBM) preparation. Arch Oral Biol 2012;57:1264–73.
[48] Dong X, Wang Q, Wu T, Pan H. Understanding adsorption-desorption dynamics of BMP-2 on hydroxyapatite (001) surface. Biophys J 2007;93:750–9.
[49] Boix T, Gómez-Morales J, Torrent-Burgués J, Monfort A, Puigdomènech P, Rodríguez-Clemente R. Adsorption of recombinant human bone morphogenetic protein rhBMP-2m onto hydroxyapatite. J Inorg Biochem 2005;99:1043–50.
[50] Surmenev RA, Surmeneva MA, Ivanova AA. Significance of calcium phosphate coatings for the enhancement of new bone osteogenesis—a review. Acta Biomater 2014;10:557–79.
[51] Yamaguchi M. Role of nutritional zinc in the prevention of osteoporosis. Mol Cell Biochem 2010;338:241–54.
[52] Dumas JE, BrownBaer PB, Prieto EM, Guda T, Hale RG, Wenke JC, et al. Injectable reactive biocomposites for bone healing in critical-size rabbit calvarial defects. Biomed Mater 2012;7:024112.
[53] Pilia M, Guda T, Appleford M. Development of composite scaffolds for load-bearing segmental bone defects. BioMed Res Int 2013;2013:15.
[54] Sawyer AA, Song SJ, Susanto E, Chuan P, Lam CXF, Woodruff MA, et al. The stimulation of healing within a rat calvarial defect by mPCL–TCP/collagen scaffolds loaded with rhBMP-2. Biomaterials 2009;30:2479–88.
[55] Schantz JT, Woodruff MA, Lam CX, Lim TC, Machens HG, Teoh SH, et al. Differentiation potential of mesenchymal progenitor cells following transplantation into calvarial defects. J Mech Behav Biomed Mater 2012;11:132–42.
[56] Schantz J-T, Hutmacher DW, Lam CXF, Brinkmann M, Wong KM, Lim TC, et al. Repair of calvarial defects with customised tissue-engineered bone grafts II. Evaluation of cellular efficiency and efficacy in vivo. Tissue Eng 2003;9:127–39.
[57] Yeo A, Wong WJ, Teoh S-H. Surface modification of PCL-TCP scaffolds in rabbit calvaria defects: evaluation of scaffold degradation profile, biomechanical properties and bone healing patterns. J Biomed Mater Res A 2010;93A:1358–67.